

Article

The Room Temperature Highly Sensitive Ammonia Gas Sensor Based on Polyaniline and Nitrogen-Doped Graphene Quantum Dot-Coated Hollow Indium Oxide Nanofiber Composite

Sheng-Zhe Hong, Qing-Yi Huang and Tzong-Ming Wu * 

Department of Materials Science and Engineering, National Chung Hsing University, 250 Kuo Kuang Road, Taichung 402, Taiwan; gsn30628@gmail.com (S.-Z.H.); jordan20310687@gmail.com (Q.-Y.H.)

* Correspondence: tmwu@dragon.nchu.edu.tw; Tel.: +886-4-22840500

Abstract: Hollow indium trioxide (In_2O_3) nanofibers fabricated via an effectively combined method of electrospinning and high-temperature calcination were coated with nitrogen-doped graphene quantum dots (N-GQDs) prepared by a hydrothermal process through electrostatic interaction. The N-GQD-coated hollow In_2O_3 nanofibers served as a core for the synthesis of polyaniline (PANI)/N-GQD/hollow In_2O_3 nanofiber ternary composites using in situ chemical oxidative polymerization. The chemical structure and morphology of the fabricated ternary composites were characterized using Fourier transform infrared, field-emission scanning electron microscopy, and transmission electron microscopy. The gas-sensing performances of the ternary composites were estimated by a homemade dynamic test system which was supplied with a real-time resistance acquisition platform at room temperature. The response value of the PANI/N-GQD/hollow In_2O_3 nanofiber sensor with a loading of 20 wt% N-GQD-coated hollow In_2O_3 nanofiber and an exposure of 1 ppm NH_3 was 15.2, which was approximately more than 4.4 times higher than that of the PANI sensor. This ternary composite sensor was proved to be very sensitive in the detection of NH_3 at a range of concentration between 0.6 ppm and 2.0 ppm at room temperature, which is crucial in the detection of hepatic or kidney disease in human breath. The PANI/N-GQD/hollow In_2O_3 nanofiber sensor also revealed higher selectivity and repeatability when exposed to 1.0 and 2.0 ppm NH_3 at room temperature. Because of the excellent selectivity and repeatability in the detection of 1.0 and 2.0 ppm NH_3 at room temperature achieved in this study, it is considered that the PANI/N-GQD/hollow In_2O_3 nanofiber composite sensor will be a favored gas-sensing material applied on human breath for the detection of hepatic or kidney disease.

Keywords: polyaniline; nitrogen-doped graphene quantum dot; hollow indium trioxide nanofiber; composite; ammonia gas sensor



Citation: Hong, S.-Z.; Huang, Q.-Y.; Wu, T.-M. The Room Temperature Highly Sensitive Ammonia Gas Sensor Based on Polyaniline and Nitrogen-Doped Graphene Quantum Dot-Coated Hollow Indium Oxide Nanofiber Composite. *Polymers* **2021**, *13*, 3676. <https://doi.org/10.3390/polym13213676>

Academic Editor: Yong L. Joo

Received: 29 September 2021

Accepted: 19 October 2021

Published: 25 October 2021

Publisher's Note: MDPI stays neutral with regard to jurisdictional claims in published maps and institutional affiliations.



Copyright: © 2021 by the authors. Licensee MDPI, Basel, Switzerland. This article is an open access article distributed under the terms and conditions of the Creative Commons Attribution (CC BY) license (<https://creativecommons.org/licenses/by/4.0/>).

1. Introduction

Human breath comprises various amounts of gas compounds in a range of concentration from a few ppt to thousands of ppm and a lot of humidity [1–3]. A composition change significantly depends on many issues, for example, age, gender, and health condition. A breakdown product of proteins, ammonia (NH_3), normally converted into urea via the liver and evacuated by the kidneys, reveals specific relevance to hepatic or kidney disease [3–7], and when either of these two organs collapses, the concentration of NH_3 increases from many hundred ppb when healthy up to several ppm. In accordance with a previous report, a concentration of NH_3 less than 1.1 ppm is considered to be healthy, whereas greater than 1.6 ppm is regarded as unhealthy [8]. Since the concentrations of the borderline between healthy and unhealthy are unsure, an intermediate concentration range is identified for clarity. Hence, NH_3 gas sensors are utilized to monitor the level of gas and sustain it within a specific limit.

Because electronic transfer between intrinsically conducting polymers (ICPs) and gas molecules rises as gas vapor adsorption increases, ICPs have been employed as an efficient material for sensing applications [9]. Among ICPs, polyaniline (PANI) is extensively employed for sensing applications due to its easy synthesis, exceptional doping/de-doping chemical reaction, high conductivity, outstanding environmental stability, and excellent responsivity to NH_3 [10]. The incorporation of n-type metal oxide semiconductors, such as In_2O_3 , SnO_2 , CeO_2 , CoFe_2O_4 , or carbon-based materials into ICPs can improve the sensing performances of fabricated nanocomposites [11–18]. Xue et al. reported that a PANI/carbon nanotube (CNT) composite showed enhanced sensing performance and stability at room temperature as compared to that of pure PANI [12]. Yu et al. prepared a flexible PANI/ SnO_2 nanocomposite thin-film sensor based on PANI and SnO_2 . Their study revealed that the fabricated nanocomposites showed an improved response for ammonia and benzene gas with reduced recovery time [15]. Saleh et al. prepared an ammonia gas sensor by depositing a PANI/ CeFe_2O_4 nanocomposite on flexible PET film. Their results showed excellent ammonia gas-sensing performance in the range of 1–50 ppm at room temperature [17]. Indium trioxide (In_2O_3), with high optical transparency and electrical conductivity, is widely used in liquid crystal displays and sensors [18]. Recently, Wu et al. used In_2O_3 to synthesize the PANI/graphene nanoribbon (GNR)/ In_2O_3 composites with nanostructured conformation. Their investigations showed that the sensing performance at room temperature was extensively higher than that of pure GNR and In_2O_3 porous spheres [18]. The enhanced gas-sensing properties were attributed to an increase in the electron depletion layer by formation of a p–n junction between the p-type PANI and n-type In_2O_3 .

Graphene quantum dots (GQDs), one of the zero-dimensional nanoscale carbon materials, contain a monolayer or few layers of carbon atoms in a closely packed honeycomb structure [19]. Since they are a group of graphene, GQDs show outstanding conductivity, exceptional biocompatibility, and low toxicity [20,21]. GQDs also display new occurrences attributable to quantum confinement and boundary effects and, thus, have lately received much attention [22–25]. GQDs are often used in cellular imaging, drug delivery, and photovoltaic and sensing devices. Consequently, several studies have focused on developing sensing systems for biological molecules. For example, Liu et al. [26] revealed that a fluorescent probe modified by GQDs can be used for the sensitive detection of ascorbic acid. Zhao et al. [27] investigated a GQD-based graphite electrode together with a single-stranded DNA probe for the sensitive and selective determination of many target molecules. Nevertheless, many developing topics with GQDs are critical in electrochemical sensors. According to previous investigations, doped carbon nanomaterials with heteroatoms could effectively alter their native properties, such as electronic individuality and natural features [28,29]. Nitrogen-doped GQDs (N-GQDs) have been reported to have outstanding electrocatalytic capability [30].

Besides the selection of functional materials, the dimension and structure of the sensor materials also perform a significant role in sensing performance. Consequently, numerous studies have been dedicated to this topic [31–33]. For example, Rosmalini et al. reported the preparation of filled and hollow well-aligned electrospun SnO_2 nanofibers at 150 °C used as a H_2 gas sensor [31]. Their results indicated that the granular hollow SnO_2 nanofibers exhibited the highest response. Cheng et al. prepared SnO_2 hollow nanofibers with porous structures fabricated using electrospinning and calcination procedures for outstanding gas sensor application [32]. However, as far as we know, no report on PANI, N-GQD, or hollow In_2O_3 nanofiber composites has been published.

This work describes the fabrication of a new ternary nanocomposite based on the conducting polymer PANI, hollow In_2O_3 nanofiber, and N-GQD as electrode materials used as gas sensors to detect ammonia in the concentration range of 1.0–1.6 ppm in human breath. Accordingly, the fabricated material is expected to display improved gas-sensing properties and excellent repeatability. The structure and gas-sensing properties of the synthesized composites are classified in the following discussion.

2. Materials and Methods

2.1. Materials

Aniline monomer, citric acid (CA, >98%), indium (III) nitrate hydrate ($\text{In}(\text{NO}_3)_3$, >99.9%), sulfuric acid (>98%), and urea (>98%) were obtained from Sigma-Aldrich Chemical Company (St. Louis, MO, USA). Ammonium persulfate (APS, >98%), isopropyl alcohol (>98%), and polyvinylpyrrolidone (PVP) were purchased from JT-Baker Chemical Company (Phillipsburg, NJ, USA). All chemicals were used without purification.

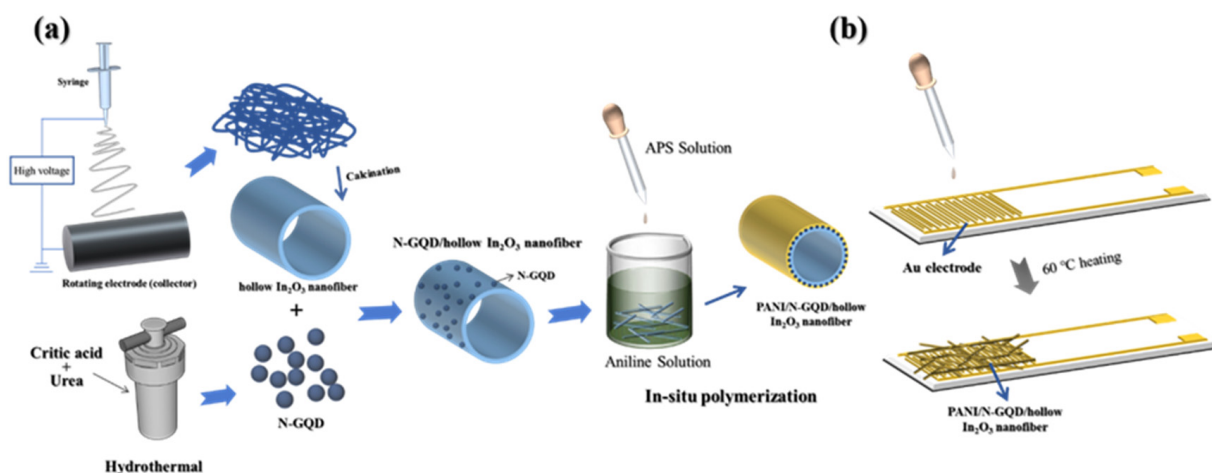
2.2. Preparation of Graphene Nanoribbon and Indium Trioxide

The N-GQDs, prepared by a hydrothermal process using urea as a nitrogen source, were synthesized according to previous reports [30,34]. First, 0.18 g urea and 0.21 g CA were mixed under stirring at room temperature for 30 min in a 10 mL beaker. Then, the mixture was transferred to a poly(tetrafluoroethylene) reactor and heated at 160 °C for 4 h. The reactants were further treated by adding ethanol to the solution and centrifuging at 5000 rpm for 2 h to obtain the N-GQD specimens. Finally, the product was washed with distilled water (DI-water) and subsequently purified by a dialysis bag for 24 h.

Indium nitrate hydrate was used as an indium source to prepare the hollow In_2O_3 nanofibers. In a typical fabrication process, 3.5 g PVP and 1.1 g $\text{In}(\text{NO}_3)_3$ were mixed in 12 mL ethyl alcohol and 10.6 mL DMF, and the solution was stirred to dissolve PVP and $\text{In}(\text{NO}_3)_3$ completely for 10 h. Then, the solution was filled into a 20 mL syringe including a 0.5 mm diameter metallic needle for electrospinning. A 20 kV high-voltage power was applied to the metallic needle tip, set at a feeding rate of 0.3 mL/h, and the distance between the needle and the collector was about 15 cm. After the 24 h electrospinning process, the obtained composite nanofibers were thermally annealed to fabricate hollow In_2O_3 nanofibers [29,32]. The thermal annealing process using calcination was operated at 800 °C for 3 h with a heating rate of 5 °C/min.

2.3. Synthesis of Polyaniline/Nitrogen-Doped Graphene Quantum Dot/Hollow Indium Trioxide Nanofiber Composites

The polyaniline (PANI)/N-GQD/hollow indium trioxide nanofiber composites were prepared using in situ chemical oxidative polymerization. Scheme 1a shows a schematic illustration of this preparation. In a typical preparation process, a certain weight ratio of N-GQD powders was dispersed in DI-water, mixed with hollow In_2O_3 nanofibers through electrostatic interaction, and sonicated for 1 h. The reactants were further treated by adding ethanol to the solution and centrifuging at 5000 rpm for 2 h to obtain the N-GQD-coated hollow In_2O_3 nanofiber specimens. Finally, the product was washed with DI-water and subsequently purified by a dialysis bag for 24 h. The obtained N-GQD/hollow In_2O_3 nanofiber was added to 50 mL HCl solution and sonicated for 2 h. After that, the aniline monomer was added to the dispersed solution of N-GQD/hollow In_2O_3 nanofiber and stirred for 1 h. Subsequently, ammonium persulfate dissolved in 20 mL HCl solution was progressively added to the mixed solution of aniline monomer/N-GQD/hollow In_2O_3 nanofiber and reacted for 3 h at 0 °C. The obtained PANI/N-GQD/hollow In_2O_3 nanofiber composite was filtered, rinsed several times with methanol and DI-water, and vacuum dried at 60 °C for 24 h. For comparison, the PANI/hollow In_2O_3 nanofiber composites were synthesized using the same method as for the PANI/N-GQD/hollow In_2O_3 nanofiber composites.



Scheme 1. The schematic illustration of (a) preparation of hollow In₂O₃ nanofibers, N-GQDs, and PANI/N-GQD/hollow In₂O₃ nanofiber composites and (b) preparation of the PANI/N-GQD/hollow In₂O₃ nanofiber sensor.

2.4. Analytical Procedures

The molecular structures of the fabricated PANI/N-GQD/hollow In₂O₃ nanofiber composites were determined by Fourier transform infrared (FTIR), Raman, and wide-angle X-ray diffraction (WAXD). FTIR spectra were determined with a PerkinElmer Spectrum One spectrometer (Waltham, Massachusetts, USA) in a range of 400–4000 cm⁻¹. Raman spectra were obtained on a Renishaw system 1000 (Renishaw Inc., West Dundee, IL, USA) using an argon ion laser performing at 514.5 nm with a CCD detector. WAXD measurement experiments were operated using an X-ray diffractometer (Bruker D8, BRUKER AXS, Inc., Madison, WI, USA) equipped with a Ni-filtered Cu K α radiation. The WAXD experiments were recorded in the range of $2\theta = 1.5^\circ\text{--}40^\circ$ with an increment of $1^\circ/\text{min}$. The morphology of all samples was classified using field-emission scanning electron microscopy (FESEM) and transmission electron microscopy (TEM). The measurement of FESEM was carried out using a JEOL JSM-6700F field-emission instrument (JEOL Ltd., Tokyo, Japan). All specimens were coated with gold to avoid charging. The measurement of TEM was carried out using JEOL JEM-2010 (JEOL Ltd., Tokyo, Japan). Samples for TEM measurement were prepared by a Reichert Ultracut ultramicrotome. The particle size distribution was obtained using a Zetasizer Nano ZS instrument (Malvern Instruments Ltd., Worcestershire, UK). The specific surface area was determined using N₂ sorption isotherms by the BET and BJH methods using a gas sorption analyzer (Quantachrome AutoSorb IQ, Montgomeryville, PA, USA).

Scheme 1b shows a schematic illustration of the sensor preparation. The gas-sensing properties of the sensors were evaluated by a homemade dynamic test system equipped with a real-time resistance acquisition platform at 25 °C and a relative humidity of $40 \pm 5\%$. The gas concentrations of NH₃ samples and interfering gas samples, including CH₃OH, C₂H₅OH, and C₃H₆O, were investigated by altering the mixing ratio of nitrogen and test samples. The sensor response is given using the equation of $R = R_g/R_a$, where R_g and R_a are the sensor resistances in test gases and air, respectively [30]. The slope of the response–concentration fitting curve is designated as the sensitivity of the sensors. The response time and recovery time were calculated as the time taken for the sensor to attain 90% of total resistance change from its initial resistance.

3. Results

Synthesis, Structure, and Morphology of PANI/N-GQD/Hollow In₂O₃ Nanofiber Composites

A characteristic TEM micrograph of N-GQDs is shown in Figure 1a. The average diameter of the N-GQDs, determined using a Nano ZS instrument, was about 6 nm (Figure 1b). Raman spectra were used to obtain the absorption bands of the N-GQDs and

are shown in Figure 1c. In this figure, two strong absorption bands at 1581 cm^{-1} (G mode) and at 1338 cm^{-1} (D mode) are observed [34].

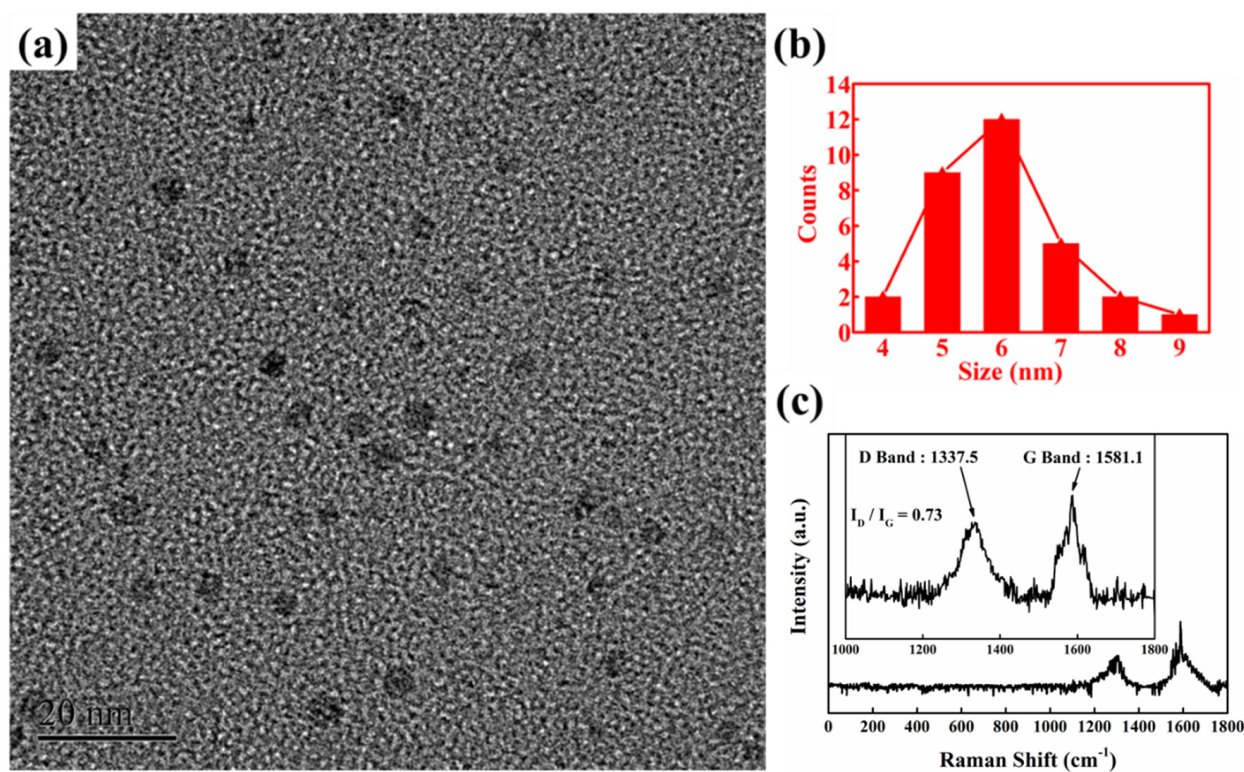


Figure 1. (a) TEM images of N-GQD, (b) particle size distribution of N-GQD, and (c) Raman spectrum of N-GQD.

The morphology and structure of the fabricated In_2O_3 nanofibers were determined using WAXD, FESEM, and TEM. Figure 2a exhibits a typical FESEM micrograph of an electrospun $\text{In}(\text{NO}_3)_3/\text{PVP}$ nanofiber, which displays a continuous fibrous morphology with smooth and uniform surfaces. The average diameter is about 540 nm. After calcination in air, the diameter of the In_2O_3 nanofibers decreased drastically to 165 nm, and the surfaces became coarse, as presented in Figure 2b. In addition, the microstructure of hollow In_2O_3 nanofibers was further identified by TEM, as illustrated in Figure 2c. The crystalline structure of the hollow In_2O_3 nanofibers was determined using a WAXD technique. The WAXD diffraction pattern of the hollow In_2O_3 nanofibers, as presented in Figure 2d, exhibits five strong diffraction peaks at $2\theta = 21.7^\circ, 30.6^\circ, 35.4^\circ, 51.2^\circ,$ and 60.7° , assigned to the (211), (222), (400), (440), and (622) crystalline planes of In_2O_3 , respectively. This finding suggests that the crystalline structure of the hollow In_2O_3 nanofibers is a cubic phase [18].

The chemical structure and morphology of the fabricated polyaniline (PANI)-coated hollow In_2O_3 nanofibers synthesized using in situ chemical oxidative polymerization were identified using the FTIR, FESEM, and TEM methods. Figure 3 shows the FTIR spectra of PANI-coated composites with various weight ratios of hollow In_2O_3 nanofiber. The FTIR data of neat PANI and hollow In_2O_3 nanofiber were also presented in this figure. The absorption peaks of hollow In_2O_3 nanofiber occurring at $538, 567,$ and 600 cm^{-1} were attributed to the In–O–In stretching vibration [35]. The characteristic peak of PANI observed at 800 cm^{-1} was attributed to the C–N^{•+} stretching vibration, and the absorption band at 1240 cm^{-1} was ascribed to a C–H out-of-plane bending vibration of the 1,4-disubstituted aromatic rings [36]. The absorption peaks at 1112 and 1294 cm^{-1} were assigned to the C=N and C–N stretching vibrations, respectively [36]. The FTIR spectra of PANI coated with significant amounts of hollow In_2O_3 nanofiber were approximately identical to those of pure PANI, indicating that the surface of the hollow In_2O_3 nanofibers was coated with PANI to form PANI/hollow In_2O_3 nanofiber composites. It was also found that the

FTIR spectra of PANI/hollow In_2O_3 nanofiber composites with higher contents of hollow In_2O_3 nanofiber show absorption peaks occurring at 538, 567, and 600 cm^{-1} , which were attributed to the In–O–In stretching vibration. This result reveals that the surface of partial hollow In_2O_3 nanofibers was not completely coated with PANI.

Figure 4 shows the FESEM and TEM images of PANI/hollow In_2O_3 nanofiber composites with various loading ratios of hollow In_2O_3 nanofibers. By adding the hollow In_2O_3 nanofiber to PANI, the diameters of the PANI/hollow In_2O_3 nanofiber composites decreased as the weight ratio of hollow In_2O_3 nanofiber increased to 20 wt%. Notably, in Figure 4a, the diameters of the PANI/hollow In_2O_3 nanofiber composites decreased from 180–200 nm to 140–160 nm for 20 wt% hollow In_2O_3 nanofiber. The decreasing diameter in the PANI/hollow In_2O_3 nanofiber composites can be attributed to the increasing weight ratio of hollow In_2O_3 nanofiber, which reduces the ratio of aniline monomer/hollow In_2O_3 nanofiber and possibly gives more active sites for the absorption and polymerization of aniline monomers on the surface of the hollow In_2O_3 nanofiber, thereby decreasing the coating thickness of PANI layers. The data of the coating thickness of the PANI layer for the PANI/hollow In_2O_3 nanofiber composites, calculated using TEM images, is listed in Table 1. As the content of hollow In_2O_3 nanofiber increases, the diameter of PANI/hollow In_2O_3 nanofiber composites slightly increases, which can be ascribed to the aggregation effect. Figure 5 shows the specific surface area of the PANI/hollow In_2O_3 nanofiber composites with various loading ratios of hollow In_2O_3 nanofiber. The data of the specific surface area for the PANI/hollow In_2O_3 nanofiber composites are also recorded in Table 1. It is clear that the specific surface area increases with the increase in weight ratio of hollow In_2O_3 nanofiber to 20 wt%. This observation is in good agreement with the FESEM/TEM images.

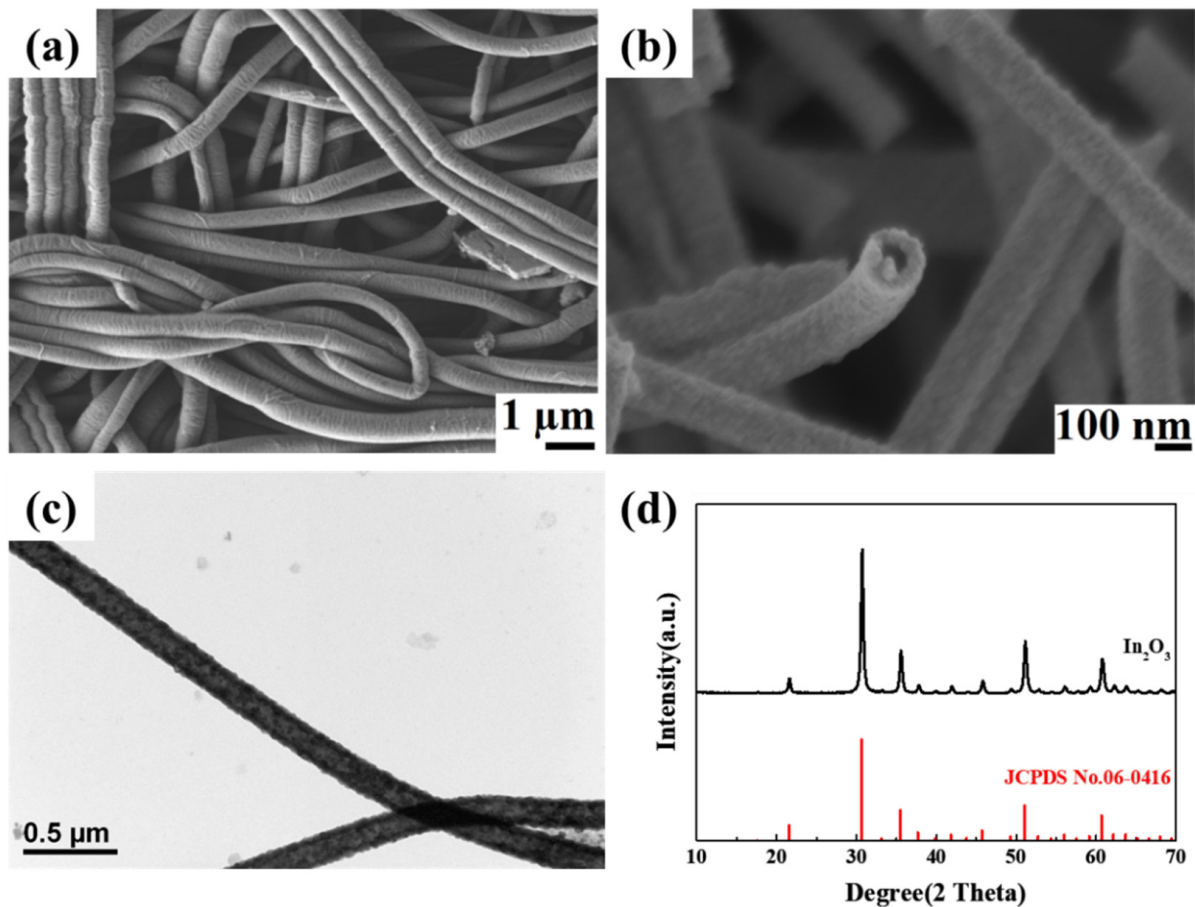


Figure 2. (a) SEM images of In_2O_3 /PVP electrospun fibers; (b) SEM images of hollow In_2O_3 nanofibers after 800 °C calcination; (c) TEM images of hollow In_2O_3 nanofibers; and (d) WAXD pattern of hollow In_2O_3 nanofibers.

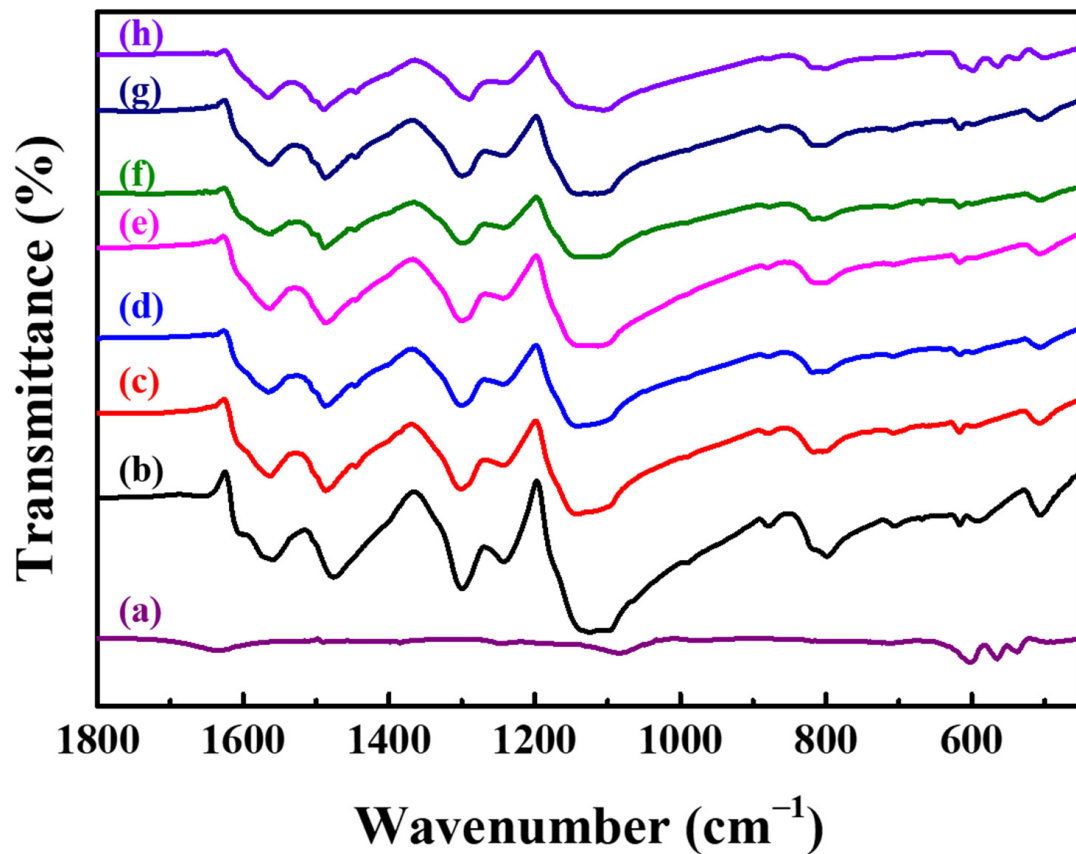


Figure 3. FTIR spectra of (a) hollow In_2O_3 nanofiber, (b) neat PANI polymer matrix, (c) 2.5 wt% PANI/hollow In_2O_3 nanofiber, (d) 5 wt% PANI/hollow In_2O_3 nanofiber, (e) 10 wt% PANI/hollow In_2O_3 nanofiber, (f) 15 wt% PANI/hollow In_2O_3 nanofiber, (g) 20 wt% PANI/hollow In_2O_3 nanofiber, and (h) 25 wt% PANI/hollow In_2O_3 nanofiber composites.

Table 1. Data of the specific surface area and the coating thickness of the PANI layer for the PANI/hollow In_2O_3 nanofiber composites.

Sample	Specific Surface Area (m^2/g)	Coating Thickness of PANI (nm)
2.5 wt% PANI/hollow In_2O_3 nanofiber	25.0	56.1
5 wt% PANI/hollow In_2O_3 nanofiber	47.7	23.7
10 wt% PANI/hollow In_2O_3 nanofiber	48.3	19.4
15 wt% PANI/hollow In_2O_3 nanofiber	69.9	17.7
20 wt% PANI/hollow In_2O_3 nanofiber	102.1	10.3
25 wt% PANI/hollow In_2O_3 nanofiber	73.5	19.6

NH_3 -sensing performance of PANI/N-GQD/hollow In_2O_3 nanofiber composites.

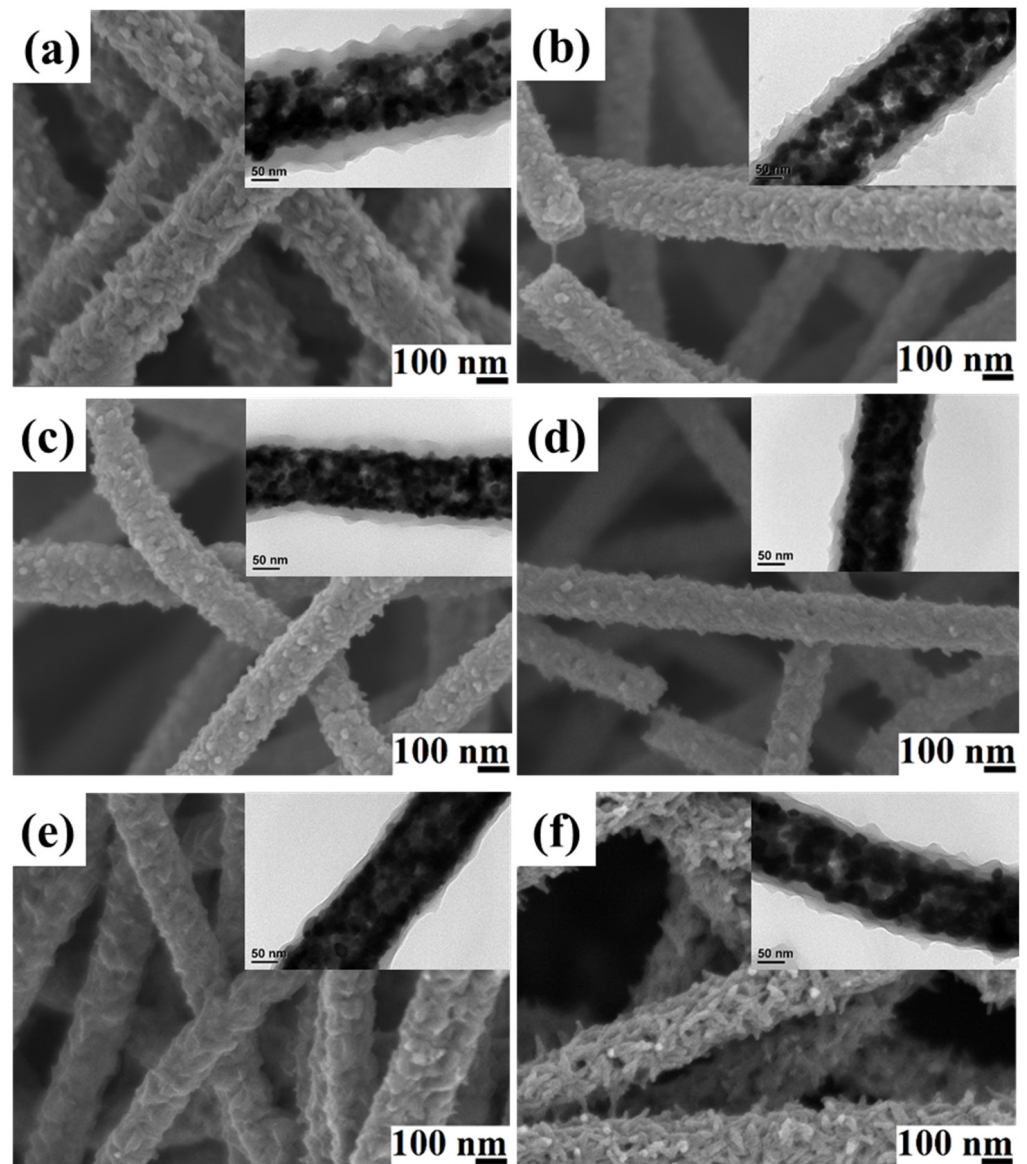


Figure 4. SEM and TEM images of (a) 2.5 wt% PANI/hollow In_2O_3 nanofiber, (b) 5 wt% PANI/hollow In_2O_3 nanofiber, (c) 10 wt% PANI/hollow In_2O_3 nanofiber, (d) 15 wt% PANI/hollow In_2O_3 nanofiber, (e) 20 wt% PANI/hollow In_2O_3 nanofiber, and (f) 25 wt% PANI/hollow In_2O_3 nanofiber composites.

The response and recovery attributes of neat PANI and various hollow In_2O_3 nanofiber ratios of PANI/hollow In_2O_3 nanofiber sensors were comparatively investigated to estimate the effect of the weight ratio of hollow In_2O_3 nanofiber on the NH_3 -sensing performance of the PANI/hollow In_2O_3 nanofiber sensor. The dynamic response–recovery curves of the composite sensors, with exposure of 1 ppm NH_3 at room temperature, are presented in Figure 6. It was observed that the PANI/hollow In_2O_3 nanofiber sensor reacted with an improvement in resistance when exposed to NH_3 and the resistance dropped down to the original state after the NH_3 was substituted with dry air. This result reveals a distinctive performance of the PANI/hollow In_2O_3 nanofiber composite film and an excellent reversibility of the PANI/hollow In_2O_3 nanofiber sensor. Particularly, the PANI/hollow In_2O_3 nanofiber sensor exhibited much higher response values than the pure PANI, indicating that the hollow In_2O_3 nanofiber plays a promising role in NH_3 -sensing measurements. It was also noticed that the PANI/hollow In_2O_3 nanofiber sensor with 20 wt% hollow In_2O_3 nanofiber loading achieved a maximum response which was far superior to other composite specimens. In order to estimate the effect of different weight ratios of hollow

In_2O_3 nanofiber on the NH_3 -sensing performance of the PANI/hollow In_2O_3 nanofiber sensor, the plot of the specific surface area, the coating thickness of the PANI layer, and the response values for the PANI/hollow In_2O_3 nanofiber composites versus the adding ratios of hollow In_2O_3 nanofiber is shown in Figure 7. It is clear that the 20 wt% hollow In_2O_3 nanofiber loaded PANI/hollow In_2O_3 nanofiber composite possesses the highest specific surface area, the smallest coating thickness of the PANI layer, and the highest response values of the PANI/hollow In_2O_3 nanofiber composites. Therefore, 20 wt% hollow In_2O_3 nanofiber loading was used as the optimal loading ratio to fabricate the PANI/N-GQD/hollow In_2O_3 nanofiber composites. Figure 8a illustrates the response of PANI, 20 wt% PANI/hollow In_2O_3 nanofiber, and 20 wt% N-GQD-coated hollow In_2O_3 PANI/N-GQD/hollow In_2O_3 nanofiber. The response value of pure PANI was about 3.6, but with the loading of 20 wt% hollow In_2O_3 nanofiber into PANI the response value was extensively enhanced to 11.2. The response value of the PANI/N-GQD/hollow In_2O_3 nanofiber sensor was 15.2 with the loading of coated N-GQD on the surface of the hollow In_2O_3 nanofiber. The improvement of the sensing performance was ascribed to the existence of a p-n junction between the p-type PANI and n-type N-GQD-coated hollow In_2O_3 nanofiber [18,36]. The sensing reversibility and repeatability of the PANI/N-GQD/hollow In_2O_3 nanofiber sensor to 1.0 ppm NH_3 are shown in Figure 8b. The response value of the PANI/N-GQD/hollow In_2O_3 nanofiber gas sensor came back to the initial response value after exposure to 1.0 ppm NH_3 . This characteristic behavior of response and recovery to 1.0 ppm NH_3 confirmed excellent reproducibility in the process of five continues cycles. This result suggests that the PANI/N-GQD/hollow In_2O_3 nanofiber sensor has good repeatability.

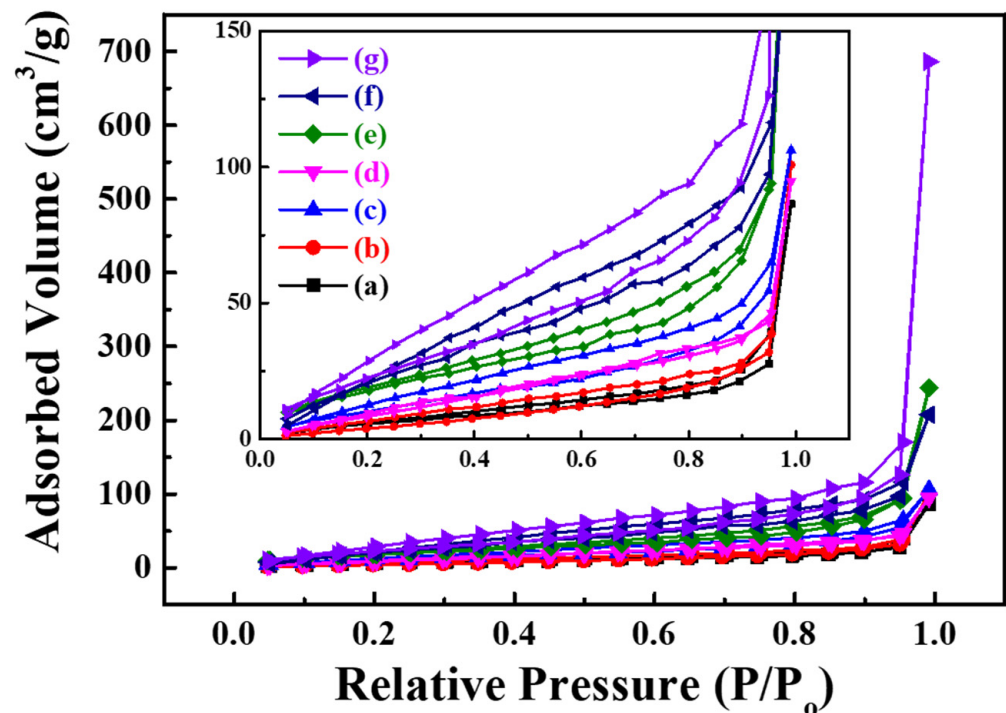


Figure 5. The BET curves of (a) neat PANI polymer matrix, (b) 2.5 wt% PANI/hollow In_2O_3 nanofiber, (c) 5 wt% PANI/hollow In_2O_3 nanofiber, (d) 10 wt% PANI/hollow In_2O_3 nanofiber, (e) 15 wt% PANI/hollow In_2O_3 nanofiber, (f) 20 wt% PANI/hollow In_2O_3 nanofiber, and (g) 25 wt% PANI/hollow In_2O_3 nanofiber composites.

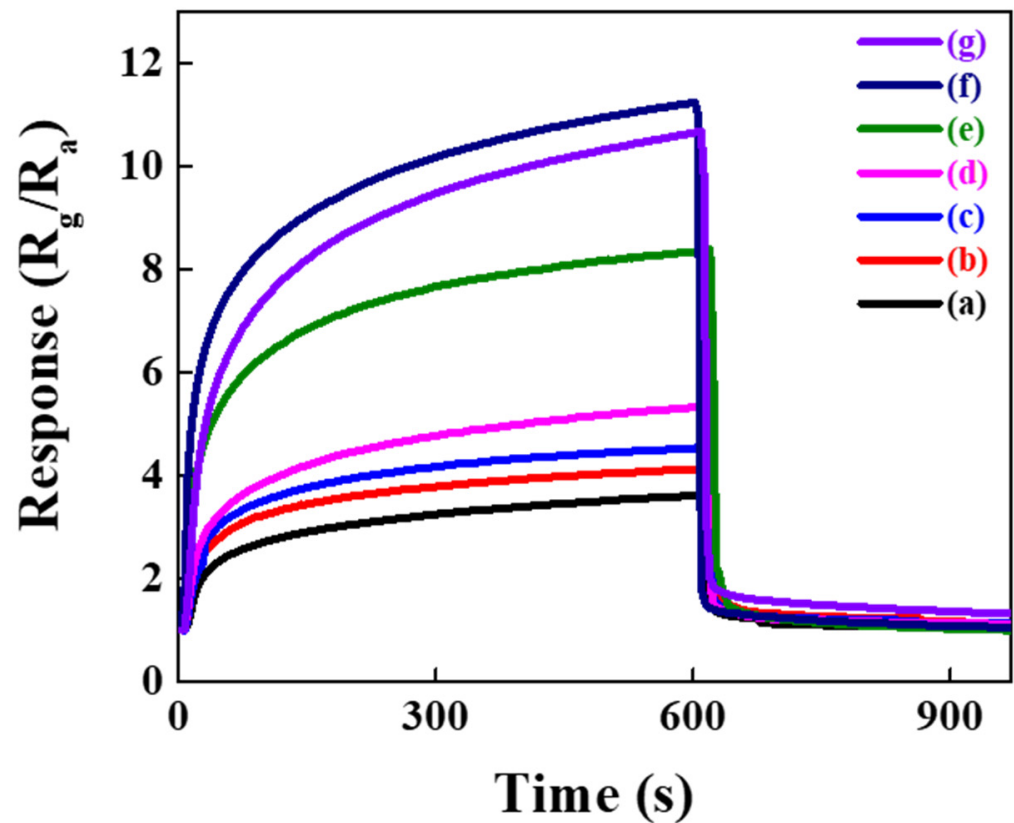


Figure 6. The response curves of (a) neat PANI polymer matrix, (b) 2.5 wt% PANI/hollow In_2O_3 nanofiber, (c) 5 wt% PANI/hollow In_2O_3 nanofiber, (d) 10 wt% PANI/hollow In_2O_3 nanofiber, (e) 15 wt% PANI/hollow In_2O_3 nanofiber, (f) 20 wt% PANI/hollow In_2O_3 nanofiber, and (g) 25 wt% PANI/hollow In_2O_3 nanofiber composites with exposure of 1 ppm NH_3 at room temperature.

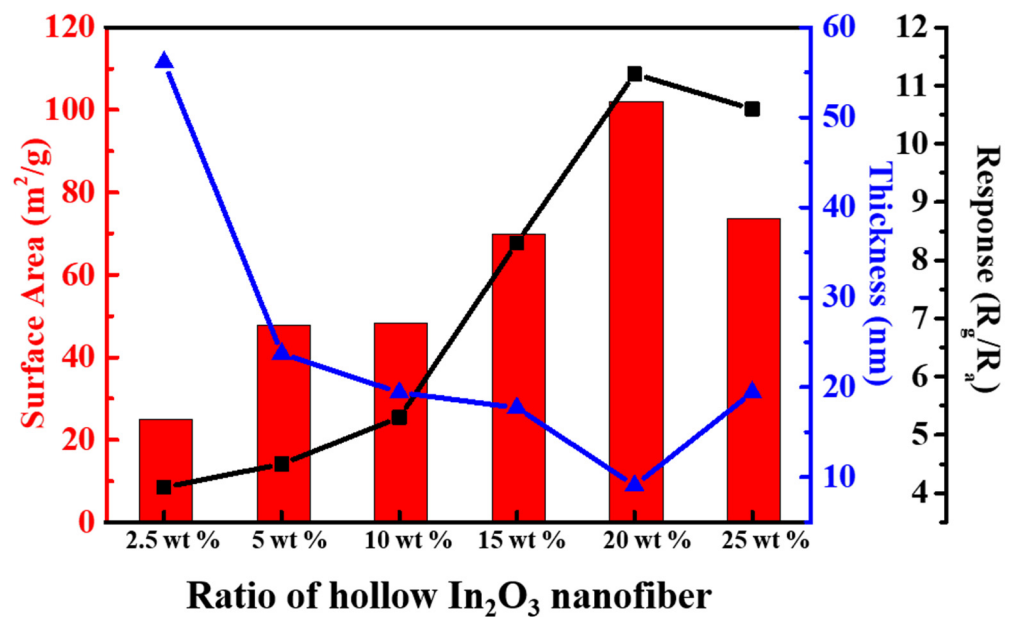


Figure 7. The surface area and thickness of PANI-coated hollow In_2O_3 nanofiber and the response versus the loading of hollow In_2O_3 nanofiber of PANI/hollow In_2O_3 nanofiber composites.

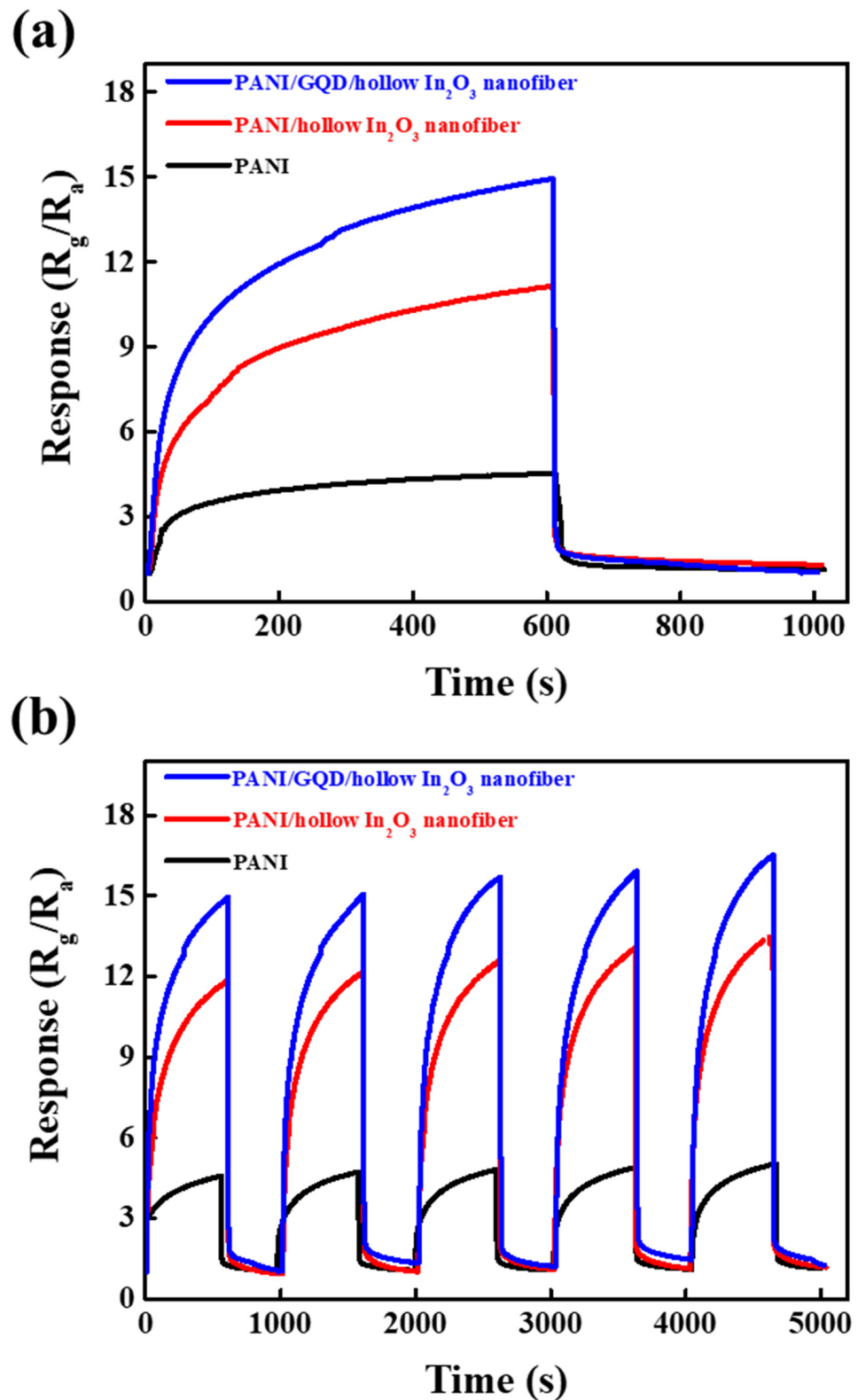


Figure 8. (a) The response curves and (b) the sensing repeatability and reversibility of neat the PANI polymer matrix, 20 wt% PANI/hollow In₂O₃ nanofiber, and 20 wt% PANI/GQD/hollow In₂O₃ nanofiber composites with exposure of 1 ppm NH₃ at room temperature.

The PANI/N-GQD/hollow In₂O₃ nanofiber sensor was applied to detect NH₃ in a concentration ranging from 0.6 ppm to 2.0 ppm at room temperature and to estimate the NH₃-sensing performance of the composite sensor used in the analysis of human breath

for hepatic or kidney disease. The NH_3 -sensing performance of the PANI/N-GQD/hollow In_2O_3 nanofiber sensor compared with the PANI and PANI/hollow In_2O_3 nanofiber sensors is shown in Figure 9a. These results indicate that the response of each sensor immediately increased as the exposure to NH_3 increased and then dropped significantly to an initial state after exposure to dry air. When the concentration of the analyte increased, the response of each sensor increased significantly. These results suggest that all responses of the three sensors had almost the same trend but the response values of the three sensors at the same concentration were exceptionally different. The response values of the PANI/N-GQD/hollow In_2O_3 nanofiber sensors were about 9.4, 11.6, 15.2, 17.4, 22.7, 28.6, 35.8, and 41.2 toward the corresponding concentrations of 0.6, 0.8, 1.0, 1.2, 1.4, 1.6, 1.8, and 2.0 ppm, respectively. It is apparent that the PANI/N-GQD/hollow In_2O_3 nanofiber sensor exhibited the highest response among the three sensors. At 1.0 ppm, the response value of the PANI/N-GQD/hollow In_2O_3 nanofiber sensor was about 4.4 and 1.4 times higher than those of the PANI and PANI/hollow In_2O_3 nanofiber sensors, respectively. Figure 10 shows the responses of the three sensors as a function of various concentrations of NH_3 . These curves reveal that the correlation between the response values and the NH_3 concentration is nearly linear. The corresponding functions were determined as $y = 2.04x + 2.55$, $y = 15.23x - 3.88$, and $y = 23.95x - 10.41$ for the PANI, PANI/hollow In_2O_3 nanofiber, and PANI/N-GQD/hollow In_2O_3 nanofiber sensors, respectively. The correlation coefficients, R^2 , were approximately equal to 0.994. The slopes of the corresponding lines, designated as the sensitivities of the sensors, reveal that the sensitivity of the PANI/N-GQD/hollow In_2O_3 nanofiber sensor was superior to those of the PANI and PANI/hollow In_2O_3 nanofiber sensors. These findings suggest that the PANI/N-GQD/hollow In_2O_3 nanofiber sensor has a greater ability to detect NH_3 , recommending it for suitable use as a favored substance for NH_3 gas detection. A comparison of the sensing performance of the PANI/N-GQD/hollow In_2O_3 nanofiber sensor and previously described devices was recorded in Table 2. It is evident that the PANI/N-GQD/hollow In_2O_3 nanofiber sensor exhibited better sensing performance to NH_3 at room temperature than previously described devices. Consequently, commingled p-type PANI and n-type N-GQD-coated hollow In_2O_3 nanofibers could be applied as an effectual approach for improving the NH_3 -sensing response of sensors.

Figure 10 presents the synergistic effect of the PANI/N-GQD/hollow In_2O_3 nanofiber ternary material, from which it is apparent that the combination of N-GQD and hollow In_2O_3 nanofibers enhances the response of PANI to NH_3 gas. PANI-coated N-GQD/hollow In_2O_3 nanofibers can generate new chemical bonds on the oxygen-containing defects of N-GQD and hollow In_2O_3 nanofiber surfaces. The extensive special surface area of N-GQDs and hollow In_2O_3 nanofibers further improves the contact sites with PANI, which can provide a considerable number of adsorption sites for NH_3 gas. This observable fact has previously been proved in Figures 4, 5 and 7. Consequently, the synergistic arrangement of N-GQD, hollow In_2O_3 nanofiber, and PANI creates exceptional sensing properties superior to those of pure PANI and PANI/hollow In_2O_3 nanofiber sensors. The characteristic of p–n heterojunctions generated between the p-type PANI and n-type N-GQD-coated hollow In_2O_3 nanofibers could be attributed as another NH_3 -sensing mechanism of the PANI/N-GQD/hollow In_2O_3 nanofiber film. The positions of the conduction band (E_c) and valence band (E_v) in In_2O_3 , the highest occupied molecular orbital (HOMO) and lowest unoccupied molecular orbital (LUMO) for PANI, and the Fermi levels (E_f) regarding the vacuum level are presented in the energy band gap structure diagram in Figure 10. The band gaps for PANI and In_2O_3 are 2.96 and 3.85 eV, respectively [15,37]. As the occurrence of the heterojunction between the p-type PANI and n-type N-GQD-coated hollow In_2O_3 nanofiber is present, a self-established electronic field of depletion layer is generated. When the sensor is subjected to NH_3 gas, the In_2O_3 electrons and PANI holes shift in opposite directions until the new Fermi level achieves equilibrium. During this procedure, electron transfer from the n-type N-GQD-coated hollow In_2O_3 nanofiber to the p-type PANI is delayed, attributable to the potential barrier, which enlarges the depletion layer thickness

and resistance of the sensor [37]. The p–n heterojunction performs as an indicator amplifier and makes it easier to effectively detect tiny quantities of NH_3 [38].

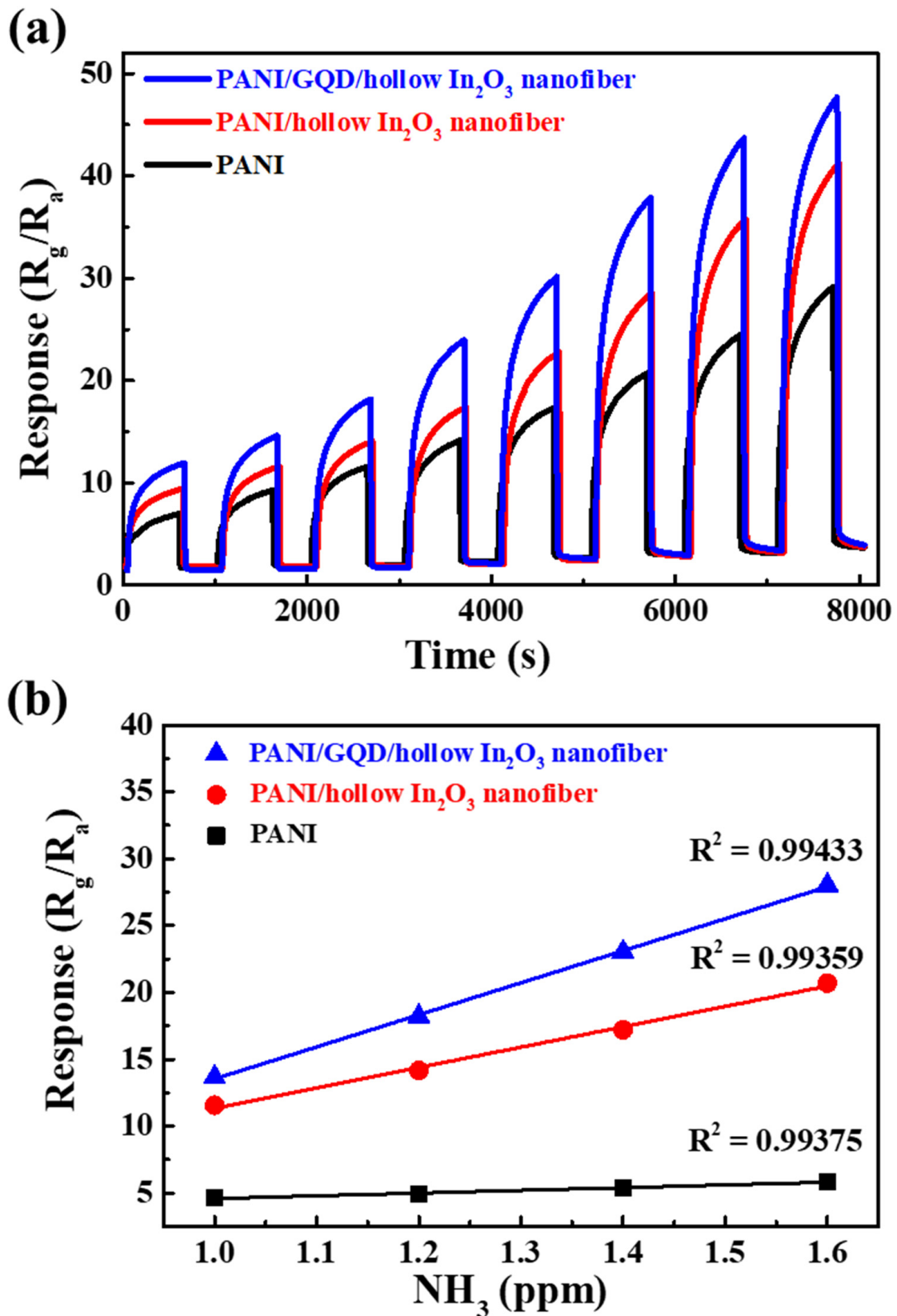


Figure 9. (a) Dynamic response–recovery curves and (b) response–concentration fitting curves of the PANI/GQD/hollow In_2O_3 nanofiber sensor.

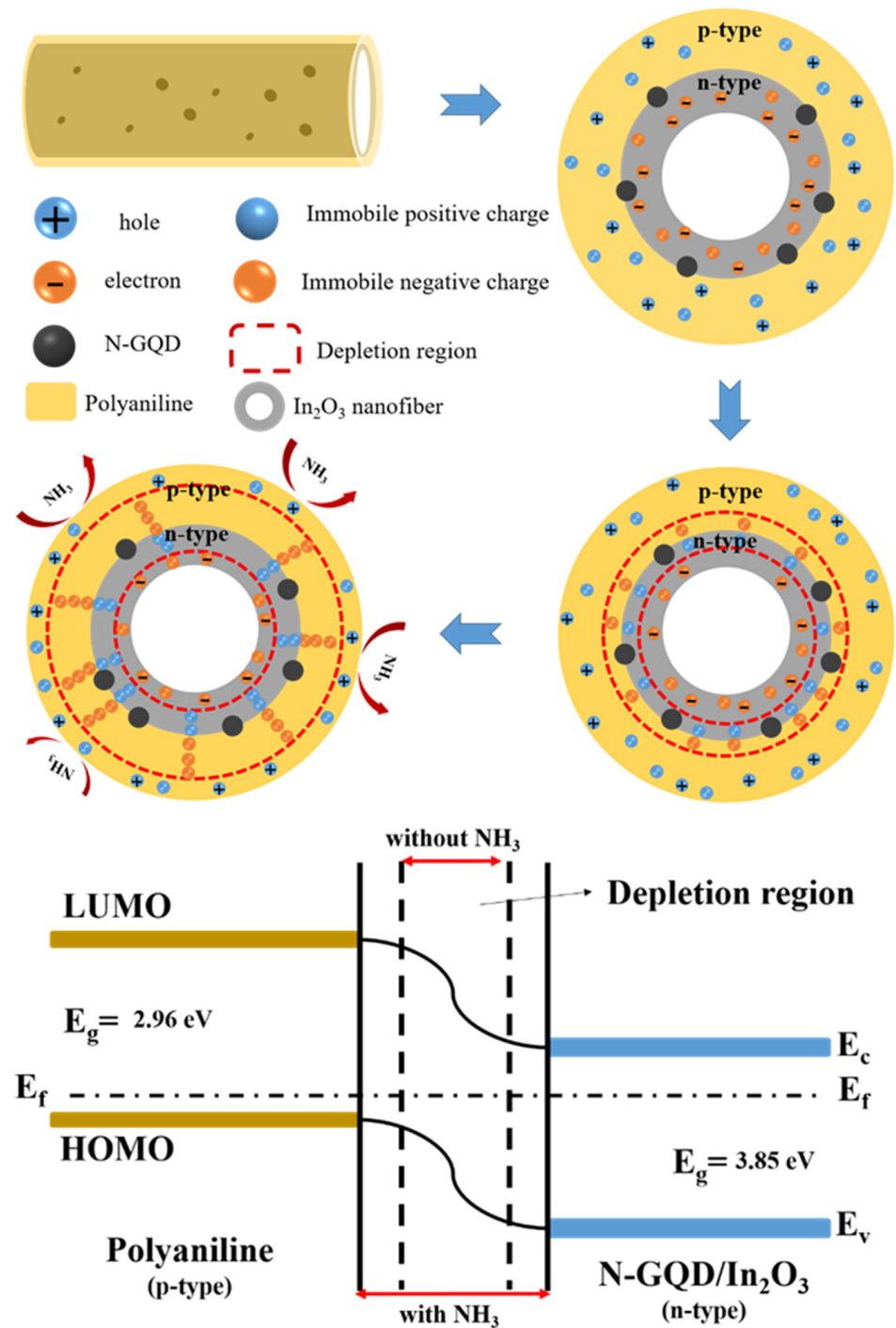
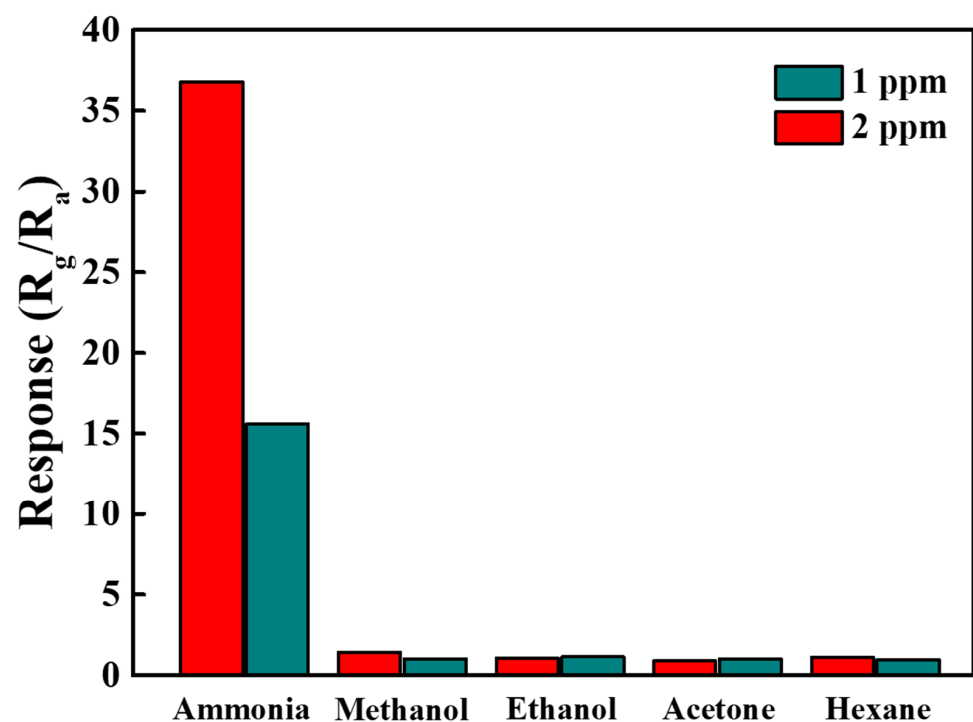


Figure 10. The schematic illustration of the sensing mechanism and energy band gap structure diagram of PANI/GQD/hollow In₂O₃ nanofiber composite sensors.

Table 2. Comparison of NH₃-sensing performance of the PANI/N-GQD/hollow In₂O₃ nanofiber sensor developed here with other sensors reported recently.

Materials	Gas	Conc. (ppm)	Temp. (°C)	Response (%)	Ref.
PANI/WO ₃	NH ₃	10	RT	7.14	[14]
PANI/In ₂ O ₃	NH ₃	100	RT	3.2	[35]
PANI/TiO ₂ -SiO ₂	NH ₃	50	RT	10	[39]
PANI/CeFe ₂ O ₄	NH ₃	50	RT	118.3	[17]
PANI/Graphene	NH ₃	50	RT	14.6	[40]
PANI/GNR/In ₂ O ₃	NH ₃	0.65	RT	8.6	[18]
PANI/PMMA	NH ₃	1	RT	1.4	[41]
PANI/Graphene/SnO ₂	NH ₃	10	RT	2.8	[42]
PANI/MoS ₂ /SnO ₂	NH ₃	50	RT	7.5	[43]
PANI/N-GQD/hollow In ₂ O ₃ nanofiber	NH ₃	1	RT	15.6	This work

For practical applications, the repeatability, reversibility, and selectivity of synthesized gas sensors are critical. Actually, gas sensors are normally exposed to numerous analytes, and it is assumed that the target analyte is detected accurately without being influenced by other species. Figure 11 exhibits the selectivity of the PANI/N-GQD/hollow In₂O₃ nanofiber sensor toward ammonia (NH₃), methanol (CH₃OH), ethanol (C₂H₅OH), and acetone (CH₃COCH₃) with a concentration of 1.0 and 2.0 ppm. The selectivity test shown in Figure 11 is the first test in sensor characterization. It was noticeably illustrated that the PANI/N-GQD/hollow In₂O₃ nanofiber sensor had a high-level response property to ammonia but displayed approximately no response to other gases. The mechanism of NH₃ selectivity may be related to the surface absorption of NH₃ on the interface of the PANI/N-GQD/hollow In₂O₃ nanofiber sensor. The de-doping response between NH₃ and PANI plays an important role in improving NH₃-sensing performance, leading to a selective response to NH₃ [18,34]. Subsequently, it can be established that the PANI/N-GQD/hollow In₂O₃ nanofiber sensor exhibited selectivity toward NH₃ at room temperature as against other gases.

**Figure 11.** The selectivity of the PANI/N-GQD/hollow In₂O₃ nanofiber film sensor tested at the concentrations of 1 and 2 ppm toward NH₃, methanol, ethanol, and acetone.

4. Conclusions

We have shown outstanding gas-sensing performances of PANI/N-GQD/hollow In₂O₃ nanofiber ternary composites effectively synthesized by in situ chemical oxidation polymerization. The response value of the 20 wt% N-GQD-coated hollow In₂O₃ nanofiber added to the PANI/N-GQD/hollow In₂O₃ nanofiber sensor was 15.1 at an exposure of 1 ppm NH₃, which was approximately 4.4 and 1.4 times higher than those of the PANI and PANI/hollow In₂O₃ nanofiber sensors, respectively. The PANI/N-GQD/hollow In₂O₃ nanofiber sensor showed the highest response at room temperature in detecting NH₃ concentrations ranging from 0.6 ppm to 2.0 ppm, as compared to those of the PANI and PANI/hollow In₂O₃ nanofiber sensors; this is critical for detecting hepatic or kidney disease in human breath. The PANI/N-GQD/hollow In₂O₃ nanofiber sensor also showed higher repeatability and selectivity on exposure to 1.0 and 2.0 ppm NH₃ at room temperature. Owing to the exceptional repeatability and selectivity in the detection of 1.0 and 2.0 ppm NH₃ at room temperature reported in this study, it is considered that the PANI/N-GQD/hollow In₂O₃ nanofiber composite sensor will be a favored gas-sensing material for the detection of hepatic or kidney disease in human breath.

Author Contributions: Conceptualization, S.-Z.H. and T.-M.W.; methodology, T.-M.W.; software, S.-Z.H. and Q.-Y.H.; validation, S.-Z.H. and Q.-Y.H.; formal analysis, S.-Z.H. and Q.-Y.H.; investigation, S.-Z.H. and Q.-Y.H.; resources, S.-Z.H.; data curation, S.-Z.H. and Q.-Y.H.; writing—original draft preparation, S.-Z.H. and Q.-Y.H.; writing—review and editing, T.-M.W.; visualization, T.-M.W.; supervision, T.-M.W.; project administration, T.-M.W.; funding acquisition, T.-M.W. All authors have read and agreed to the published version of the manuscript.

Funding: This research was funded by the Ministry of Science and Technology (MOST), Taiwan under Grant MOST 109-2212-E-005-069-MY3. The APC was funded by the Ministry of Science and Technology, Taiwan.

Institutional Review Board Statement: Not applicable.

Informed Consent Statement: Not applicable.

Data Availability Statement: Not applicable.

Acknowledgments: The financial support of this work was provided by the Ministry of Science and Technology (MOST) under Grant MOST 109-2212-E-005-069-MY3 and the Ministry of Education under the project of the Innovation and Development Center of Sustainable Agriculture (IDCSA).

Conflicts of Interest: The authors declare no conflict of interest.

References

1. Phillips, M.; Herrera, J.; Krishnan, S.; Zain, M.; Greenberg, J.; Cataneo, R.N. Variation in volatile organic compounds in the breath of normal humans. *J. Chromatogr. B Biomed. Sci. Appl.* **1999**, *729*, 75–88. [[CrossRef](#)]
2. Phillips, M.; Cataneo, R.N.; Cummin, A.R.C.; Gagliardi, A.J.; Gleeson, K.; Greenberg, J.; Maxfield, R.A.; Rom, W.N. Detection of lung cancer with volatile markers in the breath. *Chest J.* **2003**, *123*, 2115–2123. [[CrossRef](#)] [[PubMed](#)]
3. Haick, H.; Broza, Y.Y.; Mochalski, P.; Ruzsanyi, V.; Amann, A. Assessment, origin, and implementation of breath volatile cancer markers. *Chem. Soc. Rev.* **2014**, *43*, 1423–1449. [[CrossRef](#)]
4. Wehinger, A.; Schmid, A.; Mechtcheriakov, S.; Ledochowski, M.; Grabmer, C.; Amann, A. Lung cancer detection by proton transfer reaction mass-spectrometric analysis of human breath gas. *Int. J. Mass Spectrom.* **2007**, *265*, 49–59. [[CrossRef](#)]
5. Capuano, R.; Santonico, M.; Pennazza, G.; Ghezzi, S.; Martinelli, E.; Roscioni, C.; Lucantoni, G.; Galluccio, G.; Paolesse, R.; Natale, C.D.; et al. The lung cancer breath signature: A comparative analysis of exhaled breath and air sampled from inside the lungs. *Sci. Rep.* **2015**, *5*, 16491. [[CrossRef](#)]
6. Grabowska-Polanowska, B.; Faber, J.; Skowron, M.; Miarka, P.; Pietrzycka, A.; Sliwka, I.; Amann, A. Detection of potential chronic kidney disease markers in breath using gas chromatography with mass-spectral detection coupled with thermal desorption method. *J. Chromatogr. A* **2013**, *1301*, 179–189. [[CrossRef](#)] [[PubMed](#)]
7. Davies, S.; Spanel, P.; Smith, D. Quantitative analysis of ammonia on the breath of patients in end-stage renal failure. *Kidney Int.* **1997**, *52*, 223–228. [[CrossRef](#)]
8. Turner, C.; Španěl, P.; Smith, D. A longitudinal study of ammonia, acetone and propanol in the exhaled breath of 30 subjects using selected ion flow tube mass spectrometry, SIFT-MS. *Physiol. Meas.* **2006**, *27*, 321–327. [[CrossRef](#)]
9. Buckley, L.K.; Collins, G.E. Conductive polymer-coated fabrics for chemical sensing. *Synth. Met.* **1996**, *78*, 93–101.

10. Ciric-Marjanovic, G. Recent advances in polyaniline research: Polymerization mechanisms, structural aspects, properties and applications. *Synth. Met.* **2013**, *177*, 1–47. [[CrossRef](#)]
11. Eising, M.; Cava, C.E.; Salvatierra, R.V.; Zarbin, A.J.G.; Roman, L.S. Doping effect on self-assembled films of polyaniline and carbon nanotube applied as ammonia gas sensor. *Sens. Actuators B Chem.* **2017**, *245*, 25–33. [[CrossRef](#)]
12. Xue, L.; Wang, W.; Guo, Y.; Liu, G.; Wan, P. Flexible polyaniline/carbon nanotube nanocomposite film-based electronic gas sensors. *Sens. Actuators B Chem.* **2017**, *244*, 47–53. [[CrossRef](#)]
13. Liu, C.; Tai, H.; Zhang, P.; Yuan, Z.; Du, X.; Xie, G.; Jiang, Y. A high-performance flexible gas sensor based on self-assembled PANI-CeO₂ nanocomposite thin film for trace-level NH₃ detection at room temperature. *Sens. Actuators B Chem.* **2018**, *261*, 587–597. [[CrossRef](#)]
14. Li, S.; Lin, P.; Zhao, L.; Wang, C.; Liu, D.; Liu, F.; Sun, P.; Liang, X.; Liu, F.; Yan, X.; et al. The room temperature gas sensor based on polyaniline@flower-like WO₃ nanocomposites and flexible PET substrate for NH₃ detection. *Sens. Actuators B Chem.* **2018**, *259*, 505–513. [[CrossRef](#)]
15. Feng, Q.; Zhang, H.; Shi, Y.; Yu, X.; Lan, G. Preparation and gas sensing properties of PANI/SnO₂ hybrid material. *Polymers* **2021**, *13*, 1360. [[CrossRef](#)]
16. Bibi, A.; Rubio, Y.R.M.; Santiago, K.S.; Jia, H.W.; Ahmed, M.M.M.; Lin, Y.F.; Yeh, J.M. H₂S-sensing studies using interdigitated electrode with spin-coated carbon aerogel-polyaniline composites. *Polymers* **2021**, *13*, 1457. [[CrossRef](#)]
17. Alharthy, R.D.; Saleh, A. A novel trace-level ammonia gas sensing based on flexible PANI-CoFe₂O₄ nanocomposite film at room temperature. *Polymers* **2021**, *13*, 3077. [[CrossRef](#)]
18. Xu, L.H.; Wu, T.M. Synthesis of highly sensitive ammonia gas sensor of polyaniline/graphene nanoribbon/indium oxide composite at room temperature. *J. Mater. Sci. Mater. Electron.* **2020**, *31*, 7276–7283. [[CrossRef](#)]
19. Zhou, X.; Ma, P.; Wang, A.; Yu, C.; Qian, T.; Wu, S.; Shen, J. Dopamine fluorescent sensors based on polypyrrole/graphene quantum dots core/shell hybrids. *Biosens. Bioelectron.* **2015**, *64*, 404–410. [[CrossRef](#)]
20. Zhu, S.; Zhang, J.; Qiao, C.; Tang, S.; Li, Y.; Yuan, W.; Li, B.; Tian, L.; Liu, F.; Hu, R. Strongly green-photoluminescent graphene quantum dots for bioimaging applications. *Chem. Commun.* **2011**, *47*, 6858–6860. [[CrossRef](#)] [[PubMed](#)]
21. Shen, J.; Zhu, Y.; Yang, X.; Li, C. Graphene quantum dots: Emergent nanolights for bioimaging, sensors, catalysis and photovoltaic devices. *Chem. Commun.* **2012**, *48*, 3686–3699. [[CrossRef](#)]
22. Li, L.S.; Yan, X. Colloidal graphene quantum dots. *J. Phys. Chem. Lett.* **2010**, *1*, 2572–2576. [[CrossRef](#)]
23. Peng, J.; Gao, W.; Gupta, B.K.; Liu, Z.; Romero-Aburto, R.; Ge, L.; Song, L.; Alemany, L.B.; Zhan, X.; Gao, G.; et al. Graphene quantum dots derived from carbon fibers. *Nano Lett.* **2012**, *12*, 844–849. [[CrossRef](#)]
24. Tang, L.; Ji, R.; Cao, X.; Lin, J.; Jiang, H.; Li, X.; Teng, K.S.; Luk, C.M.; Zeng, S.; Hao, J. Deep ultraviolet photoluminescence of water-soluble self-passivated graphene quantum dots. *ACS Nano* **2012**, *6*, 5102–5110. [[CrossRef](#)] [[PubMed](#)]
25. Zhou, C.; Jiang, W.; Via, B.K. Facile synthesis of soluble graphene quantum dots and its improved property in detecting heavy metal ions. *Colloids Surf. B Biointerfaces* **2014**, *118*, 72–76. [[CrossRef](#)] [[PubMed](#)]
26. Liu, J.J.; Chen, Z.T.; Tang, D.S.; Wang, Y.B.; Kang, L.T.; Yao, J.N. Graphene quantum dots-based fluorescent probe for turn-on sensing of ascorbic acid. *Sens. Actuators B Chem.* **2015**, *212*, 214–219. [[CrossRef](#)]
27. Zhao, J.; Chen, G.; Zhu, L.; Li, G. Graphene quantum dots-based platform for the fabrication of electrochemical biosensors. *Electrochem. Commun.* **2011**, *13*, 31–33. [[CrossRef](#)]
28. Liu, H.T.; Liu, Y.Q.; Zhu, D.B. Chemical doping of graphene. *J. Mater. Chem.* **2011**, *21*, 3335–3345. [[CrossRef](#)]
29. Gong, K.P.; Du, F.; Xia, Z.H.; Durstock, M.; Dai, L.M. Nitrogen-doped carbon nanotube arrays with high electrocatalytic activity for oxygen reduction. *Science* **2009**, *323*, 760. [[CrossRef](#)]
30. Li, Y.; Zhao, Y.; Cheng, H.; Hu, Y.; Shi, G.; Dai, L.; Qu, L. Nitrogen-doped graphene quantum dots with oxygen-rich functional groups. *J. Am. Chem. Soc.* **2012**, *134*, 15–18. [[CrossRef](#)]
31. Kadir, R.A.; Li, Z.; Sadek, A.Z.; Rani, R.A.; Zoolfakar, A.S.; Field, M.R.; Ou, J.Z.; Chrimes, A.F.; Kalantarzadeh, K. Electrospun granular hollow SnO₂ nanofibers hydrogen gas sensors operating at low temperatures. *J. Phys. Chem. C* **2014**, *118*, 3129–3139. [[CrossRef](#)]
32. Cheng, L.; Ma, S.Y.; Li, X.B.; Luo, J.; Li, W.Q.; Li, F.M.; Mao, Y.Z.; Wang, T.T.; Li, Y.F. Highly sensitive acetone sensors based on Y-doped SnO₂ prismatic hollow nanofibers synthesized by electrospinning. *Sens. Actuators B Chem.* **2014**, *200*, 181–190. [[CrossRef](#)]
33. Hsieh, C.H.; Xu, L.H.; Wang, J.M.; Wu, T.M. Fabrication of polypyrrole/tin oxide/graphene nanoribbon ternary nanocomposite and its high-performance ammonia gas sensing at room temperature. *Mater. Sci. Eng. B* **2021**, *272*, 115317. [[CrossRef](#)]
34. Hsu, W.F.; Wu, T.M. Electrochemical sensor based on conductive polyaniline coated hollow tin oxide nanoparticles and nitrogen doped graphene quantum dots for sensitively detecting dopamine. *J. Mater. Sci. Mater. Electron.* **2019**, *30*, 8449–8456. [[CrossRef](#)]
35. Pang, Z.; Nie, Q.; Wei, A.; Yang, J.; Huang, F.; Wei, Q. Effect of In₂O₃ nanofiber structure on the ammonia sensing performances of In₂O₃/PANI composite nanofibers. *J. Mater. Sci.* **2017**, *52*, 686–695. [[CrossRef](#)]
36. Zhang, D.; Wu, Z.; Li, P.; Zong, X.; Dong, G.; Zhang, Y. Facile fabrication of polyaniline/multi-walled carbon nanotubes/molybdenum disulfide ternary nanocomposite and its high-performance ammonia-sensing at room temperature. *Sens. Actuators B Chem.* **2018**, *258*, 895–905. [[CrossRef](#)]
37. Pang, Z.; Yang, Z.; Chen, Y.; Zhang, J.; Wang, Q.; Huang, F.; Wei, Q. A room temperature ammonia gas sensor based on cellulose/TiO₂/PANI composite nanofibers. *Colloids Surf. A Physicochem. Eng. Asp.* **2016**, *494*, 248–255. [[CrossRef](#)]

38. Liu, Y.; Hao, L.; Gao, W.; Xue, Q.; Guo, W.; Wu, Z.; Lin, Y.; Zeng, H.; Zhu, J.; Zhang, W. Electrical characterization and ammonia sensing properties of MoS₂/Si *p-n* junction. *J. Alloys Compd.* **2015**, *631*, 105–110. [[CrossRef](#)]
39. Pang, Z.; Yu, J.; Li, D.; Nie, Q.; Zhang, J.; Wei, Q. Free-standing TiO₂-SiO₂/PANI composite nanofibers for ammonia sensors. *J. Mater. Sci. Mater. Electron.* **2017**, *29*, 3576–3583. [[CrossRef](#)]
40. Wei, J.; Liang, B.; Cao, Q.; Mo, C.; Zheng, Y.; Ye, X. Vertically aligned PANI nanorod arrays grown on graphene oxide nanosheets for a high-performance NH₃ gas sensor. *RSC Adv.* **2017**, *7*, 33510–33520. [[CrossRef](#)]
41. Zhang, H.D.; Tang, C.C.; Long, Y.Z.; Huang, R.; Li, J.J.; Gu, C.Z. High-sensitivity gas sensors based on arranged polyaniline/PMMA composite fibers. *Sens. Actuators A Phys.* **2014**, *219*, 123–127. [[CrossRef](#)]
42. Bera, S.; Kundu, S.; Khan, H.; Jana, S. Polyaniline coated graphene hybridized SnO₂ nanocomposite: Low temperature solution synthesis, structural property and room temperature ammonia gas sensing. *J. Alloys Compd.* **2018**, *744*, 260–270. [[CrossRef](#)]
43. Liu, A.; Lv, S.; Jiang, L.; Liu, F.; Zhao, L.; Wang, J.; Hu, X.; Yang, Z.; He, J.; Wang, C.; et al. The gas sensor utilizing polyaniline/MoS₂ nanosheets/SnO₂ nanotubes for the room temperature detection of ammonia. *Sens. Actuators B Chem.* **2021**, *332*, 129444. [[CrossRef](#)]